AUIQ Complementary Biological System
ISSN: 3007-973X
Journal homepage:
https://acbs.alayen.edu.iq

Volume 2 | Issue 1 Article 5

Thermal Carbonization of Biomass Wood Dust and Algae Wastes *via* Microwave-Assisted H_3PO_4: Desirability Function and Statistical Optimization

Raja Razuan Raja Derisa
Faculty of Applied Sciences, Universiti Teknologi MARA, 40450 Shah Alam, Selangor, Malaysia AND Advanced Biomaterials and Carbon Development (ABCD) Research Group, Faculty of Applied Sciences, Universiti Teknologi MARA, 40450, Shah Alam, Selangor, Malaysia

Hazierul F. Awang
Faculty of Applied Sciences, Universiti Teknologi MARA, 40450 Shah Alam, Selangor, Malaysia AND Advanced Biomaterials and Carbon Development (ABCD) Research Group, Faculty of Applied Sciences, Universiti Teknologi MARA, 40450, Shah Alam, Selangor, Malaysia

Muhammad Hakim Azman
Faculty of Applied Sciences, Universiti Teknologi MARA, 40450 Shah Alam, Selangor, Malaysia

Intan Nur Hidayah Abdul Rashid
Faculty of Applied Sciences, Universiti Teknologi MARA, 40450 Shah Alam, Selangor, Malaysia

Ahmad Hapiz
Faculty of Applied Sciences, Universiti Teknologi MARA, 40450 Shah Alam, Selangor, Malaysia AND Advanced Biomaterials and Carbon Development (ABCD) Research Group, Faculty of Applied Sciences, Universiti Teknologi MARA, 40450, Shah Alam, Selangor, Malaysia

Ruihong Wu
Deparment of Chemistry, Hengshui University, 053500 Hebei Province, Hengshui, China

Abdallah Reghioua
Fac. Technology, University of El Oued, 39000 El Oued, Algeria

Zaher Mundher Yaseen
Civil and Environmental Engineering Department, King Fahd University of Petroleum & Minerals, Dhahran 31261, Saudi Arabia

Lee D. Wilson
Department of Chemistry, University of Saskatchewan, Saskatoon, SK. S7N 5C9 Canada

Recommended Citation

Raja Derisa, Raja Razuan; Awang, Hazierul F.; Hakim Azman, Muhammad; Rashid, Intan Nur Hidayah Abdul; Hapiz, Ahmad; Wu, Ruihong; Reghioua, Abdallah; Yaseen, Zaher Mundher; and Wilson, Lee D. (2025), Thermal Carbonization of Biomass Wood Dust and Algae Wastes *via* Microwave-Assisted H_3PO_4: Desirability Function and Statistical Optimization, *AUIQ Complementary Biological System*: Vol. 2: Iss. 1, 60-76.
DOI: https://doi.org/10.70176/3007-973X.1023
Available at: https://acbs.alayen.edu.iq/journal/vol2/iss1/5

AUIQ COMPLEMENTARY BIOLOGICAL SYSTEM 2 (2025) 60–76

ORIGINAL STUDY

Thermal Carbonization of Biomass Wood Dust and Algae Wastes *via* Microwave-Assisted H_3PO_4: Desirability Function and Statistical Optimization

Raja Razuan Raja Deris [a,b], Hazierul F. Awang [a,b], Muhammad Hakim Azman [a], Intan Nur Hidayah Abdul Rashid [a], Ahmad Hapiz [a,b], Ruihong Wu [c], Abdallah Reghioua [d], Zaher Mundher Yaseen [e], Lee D. Wilson [f,*]

[a] Faculty of Applied Sciences, Universiti Teknologi MARA, 40450 Shah Alam, Selangor, Malaysia
[b] Advanced Biomaterials and Carbon Development (ABCD) Research Group, Faculty of Applied Sciences, Universiti Teknologi MARA, 40450, Shah Alam, Selangor, Malaysia
[c] Deparment of Chemistry, Hengshui University, 053500 Hebei Province, Hengshui, China
[d] Fac. Technology, University of El Oued, 39000 El Oued, Algeria
[e] Civil and Environmental Engineering Department, King Fahd University of Petroleum & Minerals, Dhahran 31261, Saudi Arabia
[f] Department of Chemistry, University of Saskatchewan, Saskatoon, SK. S7N 5C9 Canada

ABSTRACT

This research utilized a carbonization procedure via microwave irradiation assisted by H_3PO_4 to generate a cost-effective adsorbent (CWDAG) from wood dust (WD) and algal (AG) biomass. The resulting CWDAG adsorbent was characterized for its methylene blue (MB) dye adsorption properties. The activation process employs 800 W microwave radiation for 15 min under a nitrogen gas (99.99%) atmosphere. Multiple techniques were employed to study the physicochemical properties of CWDAG, such as FTIR, XRD, FSEM-EDX, pH_{pzc}, and BET. Box-Behnken design (BBD) was employed to optimize the three important parameters of adsorption, as follows: **A**: CWDAG dosage (0.02–0.12 g), **B**: pH (4–10), and **C**: contact time (30–420) min. BBD results show the highest removal of MB (98.6%) was met with a contact period of 225 min, a dosage of 0.12 g/100 mL of CWDAG at pH 10. Analysis of the kinetic profiles show that MB adsorption onto CWDAG occurred via a pseudo-second order (PSO) model. Adsorption isotherm analysis at equilibrium confirm that the Freundlich and Langmuir isotherm models fit the equilibrium data with similar *goodness-of-fit* results. Based on the Langmuir model, the maximum adsorption capacity (q_{max}) of CWDAG for MB is 32.3 mg/g. The possible mechanism of MB adsorption on the CWDAG surface include several contributions such as π–π stacking, H-bonding electrostatic forces, and pore filling.

Keywords: Wood dust, Algae, Microwave, Carbonization, Methylene blue, H_3PO_4

1. Introduction

The pollution of water by pharmaceuticals, heavy metals, organic dyes, and pesticides that originate from industrial waste can harm the environment. These emissions can be attributed to various industrial sectors (e.g., food, antiseptics, plastics, textiles, cosmetics, leather, and paper), which can negatively impact aquatic habitats [1]. Among these contaminants, methylene blue (MB) dye is a carcinogenic, highly toxic, and recalcitrant pollutant that poses a risk to human health and aquatic life. Small amounts of such synthetic dyes in freshwater environments can harm aquatic life and food chains [2–7]. To reduce the adverse effect of water contamination with such mutagenic and carcinogenic organic

Received 20 January 2025; revised 4 February 2025; accepted 4 February 2025.
Available online 6 March 2025

* Corresponding author.
E-mail address: lee.wilson@usask.ca (L. D. Wilson).

https://doi.org/10.13039/501100001834

dyes [5–7] requires the treatment of wastewater before discharge into freshwater sources. A variety of techniques is generally utilized to remove organic dyes from wastewater, which includes photocatalysis [8], adsorption [9], coagulation/flocculation [10], ion exchange [11], and electrochemical degradation [12]. Secondary waste, infrastructure cost, or technical difficulty presents limitations for many treatment methods. By contrast, the adsorption technique is recognized as a highly effective approach for separating chemical contaminants from water. This is attributed to some exceptional features of adsorption that includes resistance to contaminants, capacity to be reused, minimal waste generation, affordability, and high efficacy [13]. Selection of an appropriate adsorbent is vital for ensuring the efficacy of the adsorption process. An optimal adsorbent should possess high contaminant removal efficiency, widespread accessibility, affordability and technical feasibility, especially for rural regions. Various agricultural by-products are suitable as raw materials to produce absorbent materials. These include Phoenix dactylifera stones [14], maize cob [15], palm kernel shell and coconut [16], waste palm-oil shells [17], cashew nutshell [18], Citrus limon wood [19], and coconut shell [20].

Wood dust (WD) is a biomass with porous features generated from wood production. In 2020, worldwide production of wood dust reached over 38 billion tonnes. In the past, WD was often burned and disposed of in landfills, resulting in various environmental issues, including the inefficient use of resources [21–23]. More recently, the recycling and reutilization of WD has attracted significant interest due to its renewable nature, biodegradability, and hydrophilic properties. The presence of several functional groups, including -COOH and -OH serve as active adsorption sites for chemical species with compatible functionality. The hydrophilic group in WD support its capability for the adsorption of heavy metal ions and dyes [24]. WD can be readily converted into a carbonaceous adsorbent to remove dyes from water [25]. Employing non-conventional adsorbents such as wood dust is a promising alternative biomass source for traditional physical treatment of wastewater, owing to its distinctive physico-chemical properties [26]. Various studies have specifically examined the adsorption process for various dyes (e.g., acidic, basic, reactive, and metal complex dyes) onto wood dust for different types of biomass such as beech and oak [27, 28].

Multiple studies have shown that algae (AG) biomass is highly effective at removal of organic dyes and heavy metals from aqueous media [29–31]. The fibrous structure of AG and its amorphous nature of the embedded matrix of polysaccharides present in the cell wall of algae offer highly efficient biosorption capacity [32, 33]. This material was chosen for its renewability, cost-effectiveness, consistent availability throughout the year, tendency to adsorb diverse substances, and large surface area [34]. The reactive functional groups of AG include phosphate (-PO_4^{-3}), amino (-NH_2), hydroxyl (-OH), and carboxyl (-COOH) moieties, which support binding of multiple kinds of contaminants (organic and inorganic) via ion exchange and electrostatic interactions [35].

This study utilizes microwave irradiation due to its notable advantages compared to furnace heating and oven methods, including rapid heating, improved energy efficiency, and accurate energy input. As a result, the cost of energy input and time is reduced, while the output yield of carbonized products is increased [36]. Chemical activators, such as $ZnCl_2$ [37], H_2SO_4, KCl [38], H_3PO_4 [39], KOH [40], and Na_2CO_3 [41]. These activators are key components that enhance the adsorbent characteristics, which include the active area, porosity, and surface area with a mesopore structure. Consideration of the cost-effectiveness and environmental impact of phosphoric acid (H_3PO_4) provides merit for its utility as a chemical activator [42, 43].

Thus, this research aims to create and examine a carbonized absorbent (CWDAG) produced from blended of wood dust (WD) and algae (AG) *via* microwave radiation and H_3PO_4 as the activation agent. The performance of CWDAG adsorption was analyzed by examining its efficacy for MB dye removal. The RSM-BBD was employed in this study to optimize key adsorption parameters: CWDAG dosage, contact time, and solution pH. An extensive analysis of the adsorption mechanism was carried out to elucidate the MB binding process onto CWDAG.

2. Materials and methods

2.1. Materials

A wood processing factory in Shah Alam, Malaysia provided the wood dust (WD). R&M chemicals in Malaysia provided the reagents used in this study such as sodium chloride (NaCl), phosphoric acid (H_3PO_4), hydrochloric acid (HCl), hydroxide (NaOH), and methylene blue (MB) with a MW of 319.86 g/mol, and a λ_{max} of 661 nm. The algae powder (AG) used in this study was received from Shanghai Sinopharm Chemicals in China.

2.2. Preparation process of CWDAG

The wood dust (WD) biomass impurities were removed by washing with hot filtered water. Then, the samples of WD were dried for 24 h at 100 ˚C in an

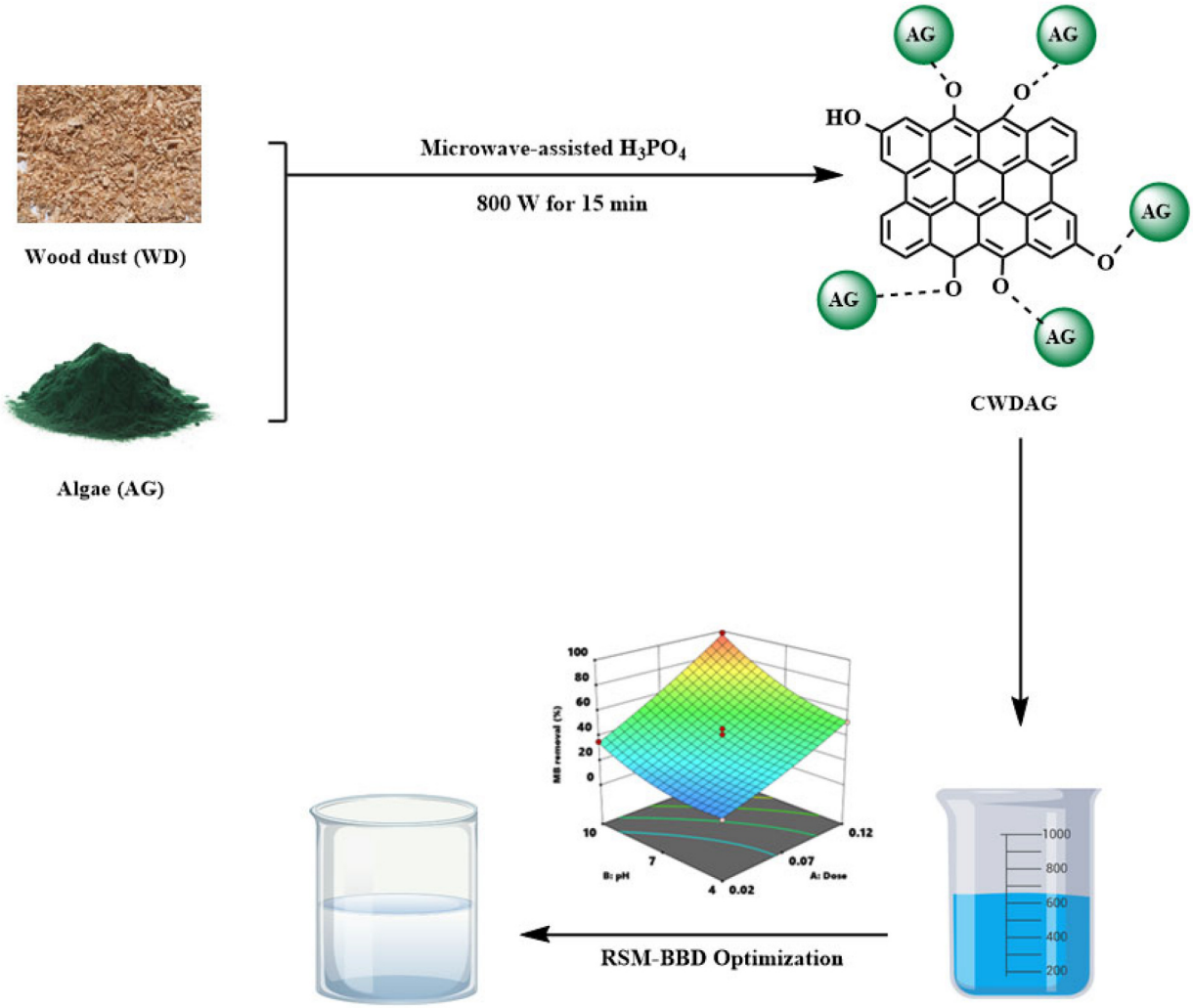

Fig. 1. Synthetic scheme for the preparation of CWDAG.

oven. The wood dust (WD) was transformed into uniformly sized (2 mm) particles by grinding and sieving, followed by mixing with algae (AG). The weight ratio of 1 g WDAG was comprised of 50% WD and 50% AG, which was used during activation by combining 2 g of H_3PO_4 as the chemical activator [44]. The microwave irradiation facilitated the carbonization process as depicted in Fig. 1. The complete drying of blended WDAG/H_3PO_4 was done by heating for 24 h at 100 ˚C in an oven. Then, the WDAG/H_3PO_4 was placed in a microwave oven (Samsung ME711K) and irradiated for 15 min at 800 watts in an inert environment of pure nitrogen (99.99%). The flow rate (100 mL/min) flow rate was constant. The produced CWDAG was then cleansed using distilled water until a neutral pH level was reached. Afterward, CWDAG was put in an oven at 100 ˚C for 24 h for the next drying stage, and then sieved with a 250 μm mesh to generate an homogeneous particle size. The powder of CWDAG was stored in a sealed container for future use.

2.3. Characterization

The phase of crystalline of CWDAG was investigated with an X-ray polycrystal diffractometer (XRD) in the range of 10° to 90°. The surface area and pore volume of CWDAG was measured using BET analysis using (Micromeritics ASAP 2060). The surface charge of CWDAG was calculated using the point of zero charge (pH_{pzc}) technique [45]. The functional group in CWDAG before and after MB adsorption employed a Fourier transform infrared (FTIR) spectrometer (Perkin-Elmer, Spectrum RX I) over a fixed spectral range of 4000–450 cm^{-1}.

Table 1. Codes and actual variables and their levels in BBD.

Codes	Variables	Level 1 (−1)	Level 2 (0)	Level 3 (+1)
A	CWDAG dose (g)/100 mL	0.02	0.07	0.12
B	pH	4	7	10
C	Time (min)	30	225	420

Table 2. Experimental matrix based on BBD approach for the design of experiments and the corresponding response (MB removal; %).

Run	Dose (g/100 mL)	pH	Time (min)	MB removal (R; %)
1	0.02	4	225	13.3
2	0.12	4	225	51.5
3	0.02	10	225	35.5
4	0.12	10	225	98.6
5	0.02	7	30	4.1
6	0.12	7	30	41.3
7	0.02	7	420	34.9
8	0.12	7	420	96.7
9	0.07	4	30	23.3
10	0.07	10	30	34.3
11	0.07	4	420	44.5
12	0.07	10	420	95.1
13	0.07	7	225	38.6
14	0.07	7	225	34.5
15	0.07	7	225	46.1
16	0.07	7	225	38.1
17	0.07	7	225	41.4

2.4. Design of adsorption experiment

The adsorption experiment was constructed using RSM-BBD with three independent parameters (CWDAG dosage, pH, and contact time). The design of BBD was constructed with the software of Stat-Ease Design Expert from Minneapolis, USA (version 13.0). The three parameters code and level are shown in Table 1. The analysis of MB dye removal was analyzed statistically using a quadratic Eq. (1).

$$Y = \beta_0 + \sum \beta_i X_i + \sum \beta_{ii} X_i^2 + \sum \sum \beta_{ij} X_i X_j \qquad (1)$$

Y is the anticipated percentage removal of MB. X_i and X_j are the independent variables that have been encoded. The term denoted by β_0 represents a specific term, whereas β_i, β_{ii}, and β_{ij} represent the coefficients for the linear, quadratic, and interaction terms of the independent variables used as inputs. Table 2 displays the output results after employing the BBD model in seventeen experiments.

2.5. Batch of adsorption study

The CWDAG adsorption capacity and percent removal of MB (R; %) were quantified to measure the effectiveness of CWDAG adsorption. The optimization results were analyzed in Table 2, where the highest removal of MB (98.6%) was reached under a contact time of 225 min, 0.12 g of CWDAG, and pH of 10. These conditions were adopted for the adsorption investigation. The water bath shaker has a constant temperature of 25°C and a fixed rate of mixing (100 rpm) in the adsorption study. The optical absorbance of MB dye was calculated using a HACH DR 3900 spectrophotometer at various concentrations, at a spectral wavelength (λ_{max}) of 661 nm. The study of MB dye removal used a MB dye concentration of 50 mg/L with a fixed volume of 100 mL, which was put in a 250 mL Erlenmeyer flask. Two kinetic models (pseudo-first order; PFO and pseudo-second order; PSO) and several equilibrium isotherm (Temkin, Langmuir, and Freundlich) models evaluated the experimental results. The adsorption profiles were obtained by using a variable MB dye concentration (20 to 250 mg/L) and time intervals (2 to 480 min). The adsorption capacity and level of color removal (%) were calculated by using Eqs. (2) and (3).

$$R\,\% = \frac{(C_o - C_e)}{C_o} \times 100 \qquad (2)$$

$$q_e = \frac{(C_o - C_e)\,V}{W} \qquad (3)$$

The dye removal (R; %) efficiency and the difference between the initial concentration (C_o) and the equilibrium concentration (C_e) of MB is expressed in milligrams per liter (mg/L). The value of R depends on the adsorption capacity (q_e) of CWDAG, expressed as mg/g. The weight of CWDAG is represented by W (g), whereas the volume of the MB solution is denoted as V (L).

3. Results and discussion

3.1. Characterization of CWDAG

The CWDAG surface area significantly influence the MB dye adsorption. Table 3 provides comprehensive data on the surface area and pore structure properties of CWDAG. The pore volume of CWDAG is 0.03 cm^3/g, and the surface area is 25.1 m^2/g. The utilization of the H_3PO_4 as an activator supports the formation of pores. The use of H_3PO_4 led to the incorporation of different polyphosphoric acid

Table 3. Physicochemical characteristics of CWDAG.

Parameters	Value
BET Surface Area (m^2/g)	25.1
Langmuir Surface Area (m^2/g)	48.3
Pore Volume (cm^3/g)	0.03
Average Pore Diameter (nm)	5.4

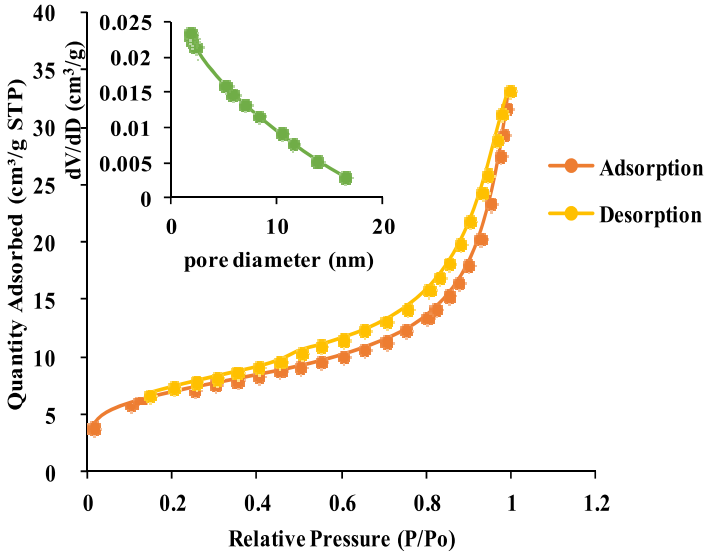

Fig. 2. The N_2 adsorption-desorption isotherms of CWDAG with the pore width distribution as the inset.

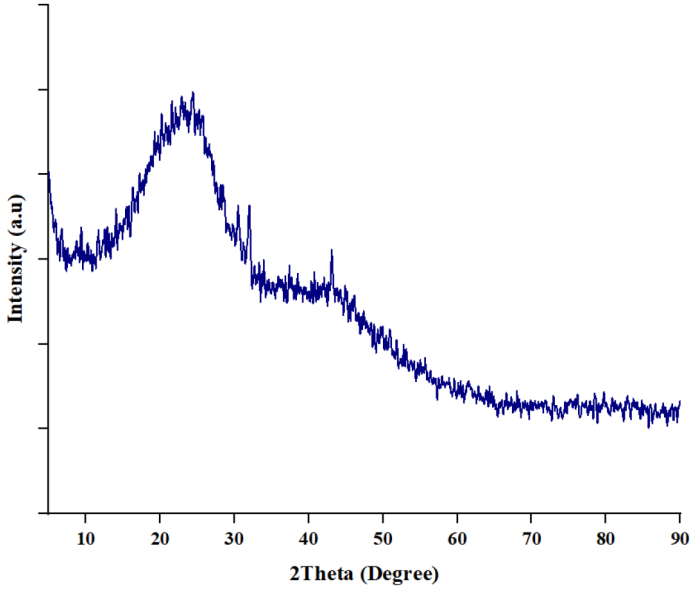

Fig. 3. XRD pattern of the CWDAG adsorbent material.

species, ranging from small ($H_4P_2O_5$) to large ($H_{13}P_{11}O_{34}$) phosphoric compounds. This synthesis yields a broader spectrum of pore sizes for CWDAG [46]. The results in Table 3 show that the CWDAG has a mesoporous structure characterized by an average pore diameter (5.4 nm) that lies between 2.0 nm to 50 nm, according to the standardized IUPAC classification [47]. Moreover, Fig. 2 depicts the N_2 adsorption and desorption isotherms for the carbonized wood-derived activated carbon (CWDAG). The isotherm indicates that the mesoporous structure of CWDAG has features of a typical Type-IV isotherm [47–49]. The BJH (Barrett, Joyner, Halenda) desorption profile supports the presence of micro and mesopore sites in CWDAG (refer to the inset in Fig. 2). As well, Fig. 2 displays a hysteresis loop categorized as H4, which signifies the presence of mesopores in the CWDAG system. The results suggest that the created CWDAG exhibits porosity with a measurable pore volume and a notable specific surface area. These results indicate the presence of a significant quantity of active sites that can effectively interact with MB dye molecules.

The phase structure of CWDAG was examined using X-ray diffraction (XRD). Fig. 3 exhibits an XRD profile of the CWDAG adsorbent, where two XRD bands at $2\theta = 15.9$ and 22.4° signify the unique structure

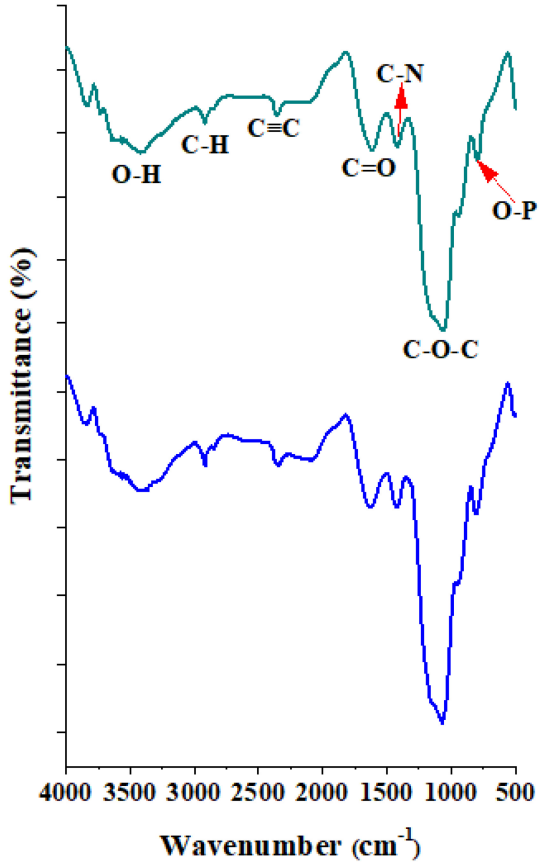

Fig. 4. FTIR spectral data: (a) CWDAG (before adsorption) and (b) CWDAG-MB (after dye adsorption).

of crystalline cellulose [50, 51]. The distinct peak observed at an angle of 24.6° [52] can determine the detection of crystalline cellulose in conjunction with AG. Additionally, Fig. 3 displays many peaks resulting from the residual ash content in CWDAG [53].

The functional groups in both CWDAG and CWDAG-MB were identified using FTIR spectral analysis, as depicted in Fig. 4(a-b). Fig. 4(a) illustrates the spectra of CWDAG, which shows adsorption bands near 3450 cm^{-1} related to the bending vibrations of O-H bonds in hemicellulose, pectin, cellulose, and lignin. The IR bands observed at 2928 cm^{-1}, 2354 cm^{-1}, 1630 cm^{-1}, 1430 cm^{-1}, 1057 cm^{-1}, and 805 cm^{-1} correspond to specific vibrational bands of chemical groupings: C-H, alkyne (C≡C), carbonyl C = O, C-N stretching, C-O-C stretching, and O-P bond vibrations, respectively [50, 54, 55]. The IR spectra of CWDAG exhibit variable peak intensity, indicating surface structure deterioration during the carbonization and thermal activation process. The FTIR spectra of CWDAG after MB adsorption reveal similar spectral features to CWDAG but with noticeable changes in specific IR bands. This trend reveals that the functional groups present in CWDAG have a role in the adsorption of MB.

The morphological characteristics and elemental content of CWDAG and CWDAG-MB were determined using an FSEM-EDX study. Fig. 5 displays scanning electron microscopy (SEM) images of CWDAG and CWDAG-MB at variable magnification (3.0k x and 5.0k x). The surface of CWDAG displays uneven, variable, and rough texture, as evidenced in Fig 5(a-b). The EDX mapping results reveal that C, O, N, and P are the main components of the CWDAG. The phosphorus content demonstrates the integration of AG into the CWDAG adsorbent structure. In addition, the morphological features of the CWDAG underwent considerable changes, becoming smoother in appearance due to the adsorption of MB onto its surface, as depicted in Fig. 5(c-d). Furthermore, EDX mapping supports the existence (C, O, N, and P) components in the CWDAG after the MB dye adsorption process.

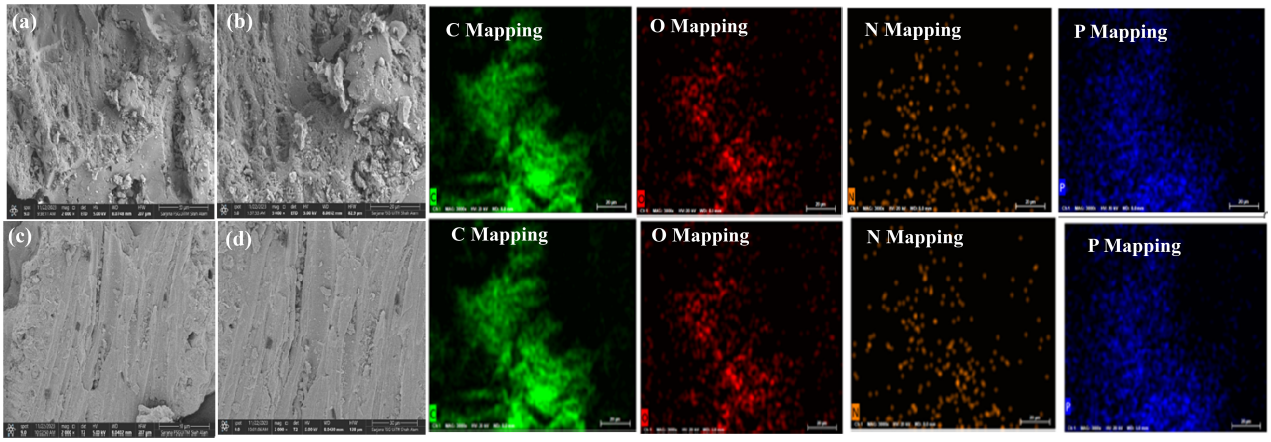

Fig. 5. FSEM images and mapping of (a-b) CWDAG and (c-d) CWDAG-MB with 5.0 k magnification, along with EDX mapping, before and after the dye adsorption process.

Table 4. ANOVA test results for MB removal by CWDAG.

Source	Sum of Squares	df	Mean Square	F-value	p-value	Remark
Model	11692.73	9	1299.19	107.08	<0.0001	Significant
A-Dose	5015.01	1	5015.01	413.34	<0.0001	Significant
B-pH	2141.85	1	2141.85	176.53	<0.0001	Significant
C-Time	3536.40	1	3536.40	291.48	<0.0001	Significant
AB	155.00	1	155.00	12.78	0.0090	Significant
AC	151.29	1	151.29	12.47	0.0096	Significant
BC	392.04	1	392.04	32.31	0.0007	Significant
A^2	25.64	1	25.64	2.11	0.1894	Not significant
B^2	237.95	1	237.95	19.61	0.0030	Significant
C^2	17.57	1	17.57	1.45	0.2680	Not significant
Residual	84.9	7	12.13			
Lack of Fit	10.28	3	3.43	0.18	0.9024	Not significant
Pure Error	74.65	4	18.66			
Cor total	11777.66	16				
R^2	0.9928					
Adjusted R^2	0.9761					

3.2. Statistical model confirmation

The model accuracy in MB removal and the suitability of the statistical data can be analyzed using Analysis of variance (ANOVA). The findings of ANOVA are presented in Table 4. According to Table 4, the F-value = 107.08 with p-value < 0.0001 suggests that the model successfully demonstrates the suitability of the model [56]. The strong agreement between the experimental and calculated data was indicated by the value of (R^2 = 0.99) [57, 58]. Typically, variables with a p-value higher than 0.05 are considered insignificant in relation to the effectiveness of the MB dye removal and vice versa. The terms A, B, C, AB, AC, BC, and B^2 in the MB dye removal model displayed statistical significance, whereas the remaining terms were insignificant. Thus, the quadratic polynomial models of the second order terms were derived by establishing a correlation between the responses (MB dye removal; %) and the tested components, as demonstrated in Eq. (4).

$$\text{MB removal } (\%) = +39.74 + 25.04A + 16.36B + 21.03C + 6.23AB + 6.15AC + 9.9BC + 7.52B^2 \quad (4)$$

In addition, the model plots validate the method used by examining the distribution of residuals, including the relative agreement between the observed and predicted values of MB dye removal. Fig. 6(a) illustrates the expected probability of the residuals for the models employed to eliminate the MB dye, where a linear data alignment suggests a consistent and uniformly distributed pattern. This alignment also indicates that the residuals are independent [59]. Fig. 6(b) illustrates the link between the experimental and theoretical values of MB dye removal. The robust association observed for the actual responses (MB dye removal) and the statistically expected values in Fig. 6(b) provide compelling evidence of the statistical validity of the models. Furthermore, Fig. 6(c) illustrates the residuals concerning the run number for MB dye removal. The data points in Fig. 6(c) exhibit a random distribution near zero, which indicates that the model is highly reliable and accurate. Moreover, the standard Box-Cox plot is used to confirm the normal distribution of the data and identify the appropriate power transformation needed to create a normal distribution for the response data when it is not normally distributed [60]. Based on the Box-Cox plot as presented in Fig. 6(d), it was determined that no transformation was required because the lambda value was close to 1 [61].

3.3. Desirability function

A desirability test is performed to compare the outcomes of experiments with the values of the prediction obtained to assess the reliability of the applied BBD model [62], as shown in Fig. 7. Fig. 7 also demonstrates the effective condition for MB removal, which requires 0.12 g/0.1 L of CWDAG dosage, pH of 9–10, and a contact time of 249 min. The projected result for CWDAG is 99%, while the experimental results for the same condition with a desirability function show that the MB dye removal onto CWDAG is 95%. The findings of this experiment reveal that the values of predicted values and the experimental results are nearly identical, confirming the reliability of the BBD model.

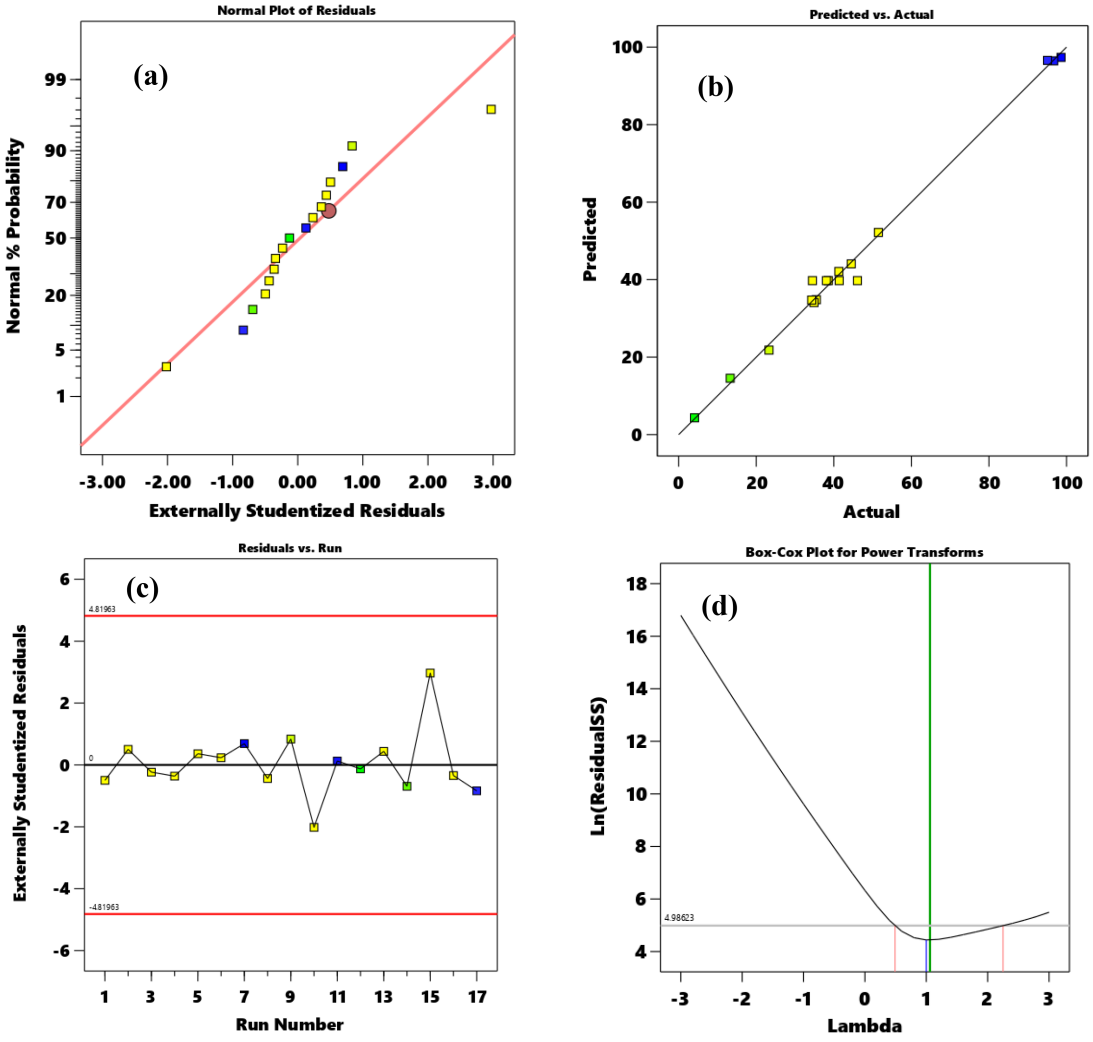

Fig. 6. BBD plots: (a) normal plot of residuals, (b) predicted vs. actual, (c) residuals vs run, and (d) Box-cox plot for MB removal by CWDAG.

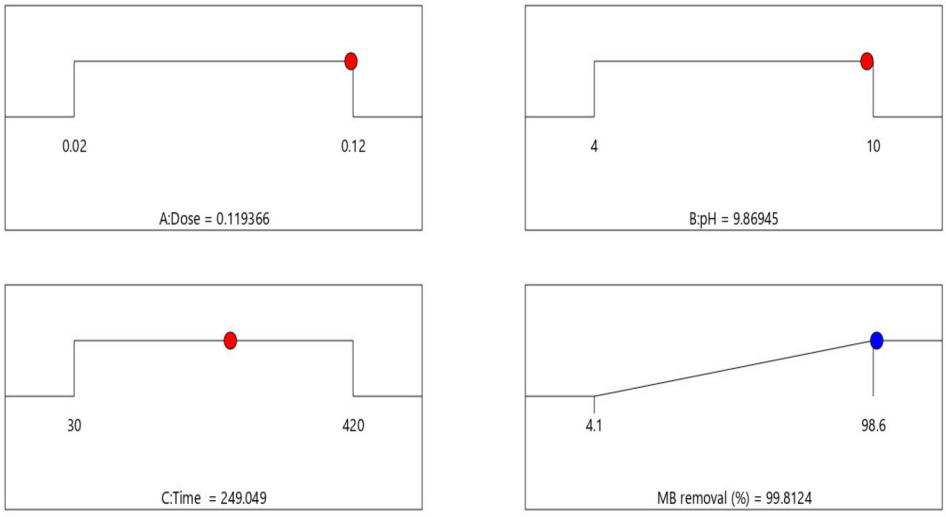

Fig. 7. (a) Desirability function of MB removal *via* CWDAG, and (b) Desirability test results.

3.4. Dual parameter impact on the removal of MB dye

The binary impact of CWDAG dosage vs pH at the constant time (225 min) was displayed in Fig. 8(a) (3D) and Fig. 8(b) (2D) plots. The results demonstrate that the MB dye removal efficiency increased as the dosage of CWDAG increased from 0.07 g to 0.12 g/0.1 L. This phenomenon correlated to the increase of active site as the surface area increased by the greater dosage of CWDAG. The 3D and 2D plots (Fig. 8(c-d)) illustrate the effect of contact time and pH on the MB removal at a constant adsorbent dose of 0.12 g. The finding shows that alkaline media (pH = 10) is the best condition for MB dye removal. This finding is correlated with the pH_{pzc} value of CWDAG (pH_{pzc} = 3.0), as indicated in Fig. 8(g). Consequently, when the pH is below pH_{pzc}, a positive surface will occur on the surface of CWDAG [63]. The findings indicate that the CWDAG surface primarily comprises negatively charged particles as the pH exceeds 3.0, which favours MB dye adsorption. The arrangement of the charged MB dye is controlled in a liquid phase when the pH value exceeds the pK_a (3.8) for the dye [64]. (Eq. (5)) shows that electrostatic interactions, at pH values greater than the pH_{pzc} of CWDAG and the pK_a of MB.

$$CWDAG - O^- + MB^+ \leftrightarrow CWDAG - O^-\ldots{}^+MB \quad (5)$$

Furthermore, Fig. 8(e-f) demonstrates the impact of different contact times and CWDAG doses on the extent of MB elimination at a constant pH of 7. Fig. 8(e-f) shows that the CWDAG displays favourable dye removal as the contact time increases from 225 to 420 min. This trend concurs with the greater occupancy of the CWDAG's active adsorption sites.

3.5. Adsorption study

The adsorption study evaluated the effectiveness of CWDAG adsorption properties with the influence of variable dye concentration (20–250 mg/L) and contact time (0–480 min) and is presented in Fig. 9. The adsorption experiment utilized a stable pH of 10 at a constant dosage of CWDAG (0.1 g). The finding of this study demonstrated the improvement of CWDAF adsorption capacity (2.40 to 29.7 mg/g) as the initial dye concentration increased from 20 to 250 mg/L. This condition yields a notable dye concentration gradient, which enhances the dye transport through the inner pores of the CWDAG to the active adsorption sites [65].

3.6. Adsorption kinetics

The greater adsorptive removal of MB using CWDAG is mainly based on the data obtained from the kinetic analysis. Kinetic models, including the PFO [66] and the PSO equations [67], which are presented in Table 5, evaluated the experimental adsorption isotherms. Table 6 details kinetic parameters obtained, where the PSO model shows higher R^2 versus the PFO model. The calculated q_e values obtained by the PSO model was relatively close to the experimentally obtained q_e values. This trend supports that the PSO model provides a favorable description of the MB dye adsorption onto CWDAG, which provide support for a chemisorption process [68].

3.7. Adsorption isotherm

The potential correlation between CWDAG and MB dye molecules can be further investigated via analysis of the isotherms. Table 5 presents the formulae for the three models, according to the Temkin [71], Freundlich [70], and Langmuir [69] isotherms. The isotherm profiles are displayed in Fig. 10, while Table 7 lists the best-fit results for these isotherms. The Freundlich and Langmuir isotherm models reveal similar *goodness-of-fit* (R^2 = 0.89–0.92) results for the adsorption of MB based on its favorable R^2 value. This validation indicates that MB can undergo multilayer adsorption onto heterogeneous surface sites of CWDAG [72]. Table 8 compares the q_{max} for CWDAG with MB (32.3 mg/g) from this study, along with results from selected literature studies. The synthesized CWDAG adsorbent reveals a capacity to absorb cationic dyes and favorable adsorption of cationic dyes such as MB from wastewater.

3.8. Dye adsorption thermodynamics

The standard difference for several thermodynamic variables, such as entropy (ΔS°), enthalpy (ΔH°), and Gibbs free energy (ΔG°) were analyzed to explain the adsorption process of MB onto CWDAG. The analysis was conducted across a temperature range (303.15 K to 333.15 K). The ΔG°, equilibrium constant (K_d), and van't Hoff Equation was calculated using equations Eqs. (6) to (8) [81, 82].

$$\Delta G^\circ = -RT\ lnK_d \quad (6)$$

$$K_d = \frac{q_e}{C_e} \quad (7)$$

$$lnK_d = \frac{\Delta S^\circ}{R} - \frac{\Delta H^\circ}{RT} \quad (8)$$

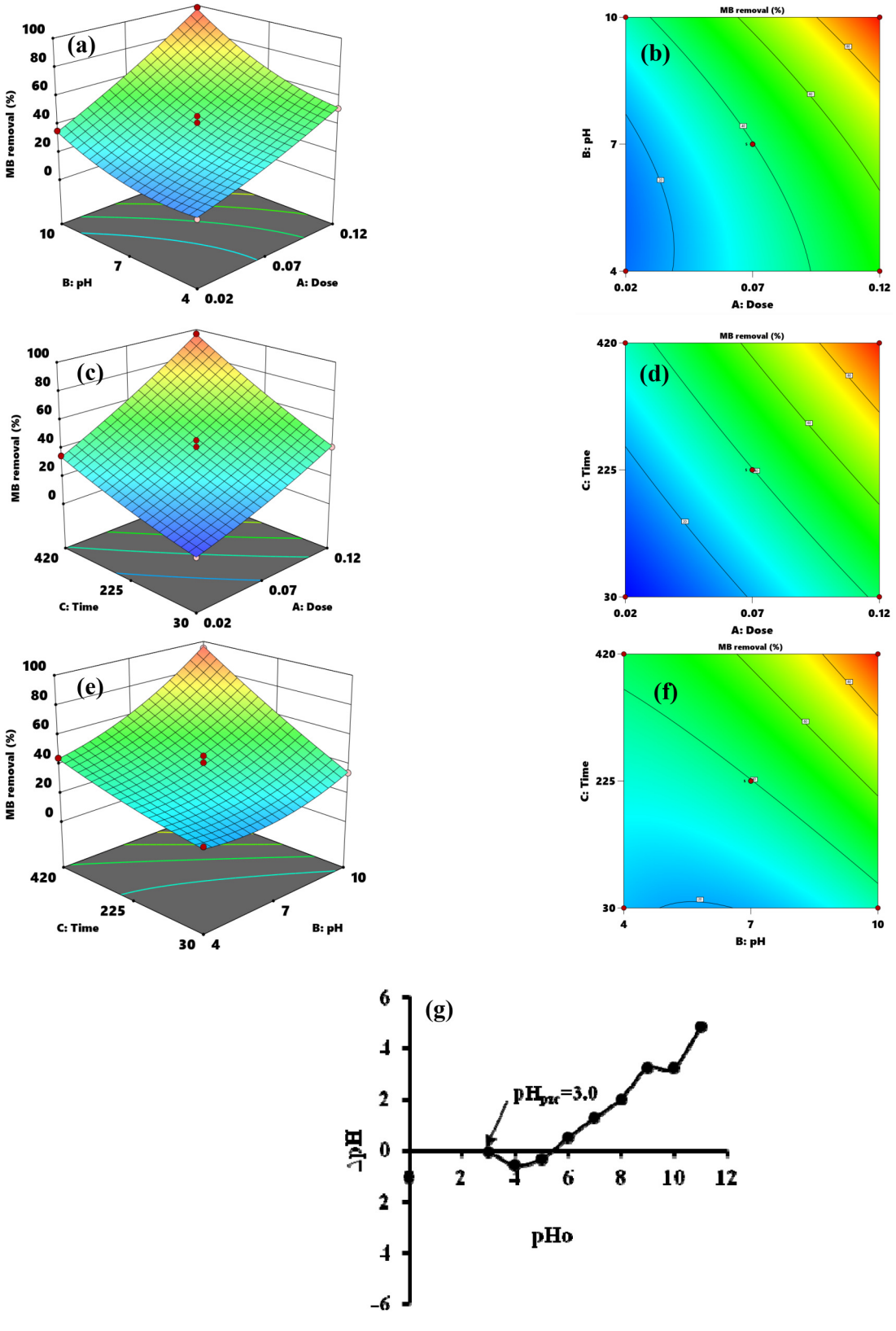

Fig. 8. 3D surface plots and 2D contour curves of the interactive impact of variable (A: dose, B: pH, and C: time) pairs (a-b) for AB while C is held constant at 225 min, (c-d) BC and A is constant at 0.12 g, (e-f) AC and B are constant at pH = 7 for MB removal response onto CWDAG, and (g) pH_{pzc} plot of CWDAG.

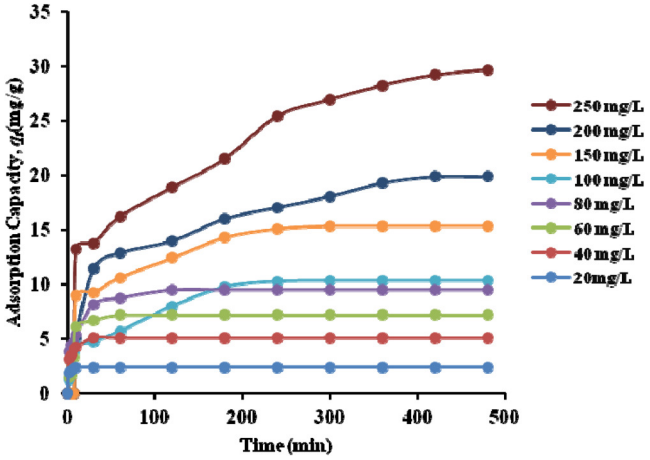

Fig. 9. Impact of initial dye concentration and kinetic adsorption profile for MB removal by the CWDAG adsorbent (dose = 0.1 g/100 mL; pH = 10, Temp = 25°C).

Table 5. Kinetic and equilibrium adsorption isotherm models.

Models	Formula	Descriptions
Pseudo-first order (PFO)	$q_t = q_e(1 - e^{-k_1 t})$	k_1: pseudo-first-order rate constant (1/min)
Pseudo-second order (PSO)	$q_t = \frac{q_e^2 k_2 t}{1 + q_e K_2 t}$	k_2: pseudo-second-order rate constant (g/mg min)
Langmuir	$q_e = \frac{q_m K_L C_e}{1 + K_L C_e}$	q_m: monolayer capacity (mg/g) K_L: Langmuir constant (L/mg)
Freundlich	$q_e = K_F C_e^{1/n}$	K_F: Freundlich constant (mg/g) (L/mg)$^{1/n}$ n: adsorption intensity
Temkin	$q_e = \frac{RT}{b_T} ln(K_T C_e)$	K_T: Temkin constant (L/mg) b_T: Heat of adsorption (J/mol)

Table 6. PFO and PSO kinetic parameters for MB adsorption onto CWDAG.

		PFO			PSO		
MB Concentration (mg/L)	$q_{e\,exp.}$ (mg/g)	$q_{e\,cal}$ (mg/g)	$k_1 \times 10$ (1/min)	R^2	$q_{e\,cal}$ (mg/g)	$k_2 \times 100$ (g/mg min)	R^2
20	2.40	2.37	6.31	0.95	2.38	86.39	0.98
40	5.20	5.00	2.74	0.94	5.12	10.60	0.98
60	7.17	7.19	0.97	0.96	7.54	1.73	0.97
80	9.44	9.23	1.10	0.94	9.62	1.72	0.97
100	10.3	9.75	0.31	0.86	10.4	0.51	0.93
150	15.4	14.9	0.26	0.92	16.7	0.18	0.95
200	19.9	18.4	0.19	0.95	21.3	0.10	0.97
250	29.7	27.4	0.02	0.92	31.7	0.06	0.95

To estimate the accompanying thermodynamic values (ΔH° and ΔS°), a plot of the natural logarithm of K_d *vs* inverse temperature (1/T) was constructed in Fig. 11. The slope of the resulting van't Hoff plot corresponds to ΔH°, whereas the y-intercept represents ΔS°. According to Table 9, the negative value of ΔG° indicates a favourable adsorption process of MB onto the CWDAG. The endothermic nature of the MB adsorption by CWDAG was verified by the value of ΔH° (+177.3 kJ/mol) [83]. The positive value for ΔS° (0.60 kJ/mol K) indicates a greater randomness at the adsorbent interface upon MB adsorption onto the CWDAG surface.

3.9. Adsorption mechanism of MB by CWDAG

A previous study showed that MB and CWDAG's interaction mechanism involved several contributions, which includes hydrogen bonding, pore-filling, π–π and electrostatic interactions [84]. Fig. 12 illustrates

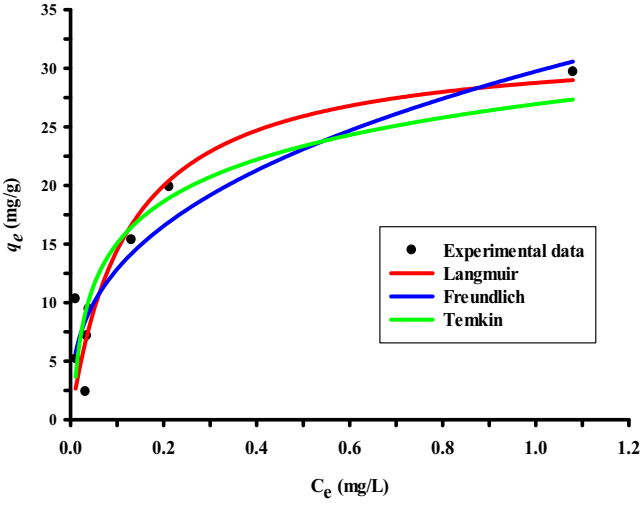

Fig. 10. Langmuir, Freundlich, and Temkin isotherm profiles for MB removal onto CWDAG (dose = 0.1 g/100 mL; pH = 10, and 25°C).

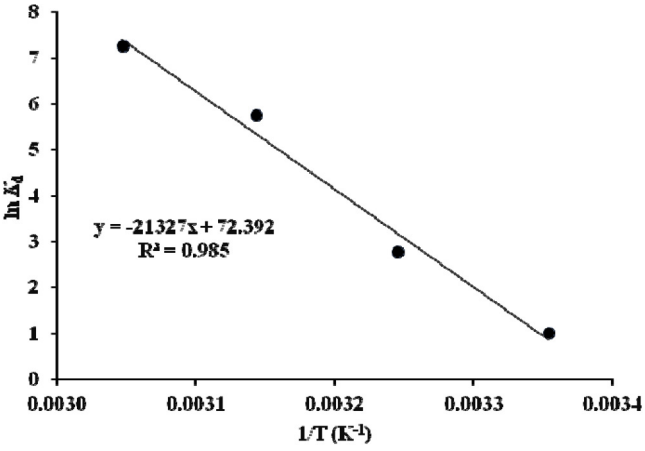

Fig. 11. A van't Hoff plot for MB removal by CWDAG (dose = 0.1 g/100 mL; pH = 10).

Table 7. Isotherm model parameters for MB removal *via* CWDAG.

Adsorption isotherm	Parameter	Value
Langmuir	q_{max} (mg/g)	32.3
	K_a (L/mg)	8.11
	R^2	0.89
Freundlich	K_f (mg/g) (L/mg)$^{1/n}$	29.7
	n	2.78
	R^2	0.92
Temkin	K_T (L/mg)	184.4
	b_T (J/mol)	487.9
	R^2	0.78

several contributions to the interaction mechanism between MB and CDWAG. The BET and SEM findings validated the pore-filling process of MB onto the mesopores of CDWAG, and the pore diameter

Table 8. Comparison of the adsorption capacity of CWDAG towards MB with different adsorbents.

Adsorbents	q_{max} (mg/g)	References
CWDAG	32.3	This study
Activated carbon derived from waste orange and lemon peels	38	[73]
Silver nanoparticles loaded on activated carbon	75.2	[74]
Carbon nanotube (CNT) incorporated eucalyptus derived activated carbon-based	49.6	[75]
Banana stem-based activated carbon	101	[76]
Bamboo waste activated carbon	285	[77]
Activated carbon from pineapple crown	292	[78]
Activated carbons from furfural residues	563	[79]
Palm-based activated carbon-alginate membrane	666	[80]

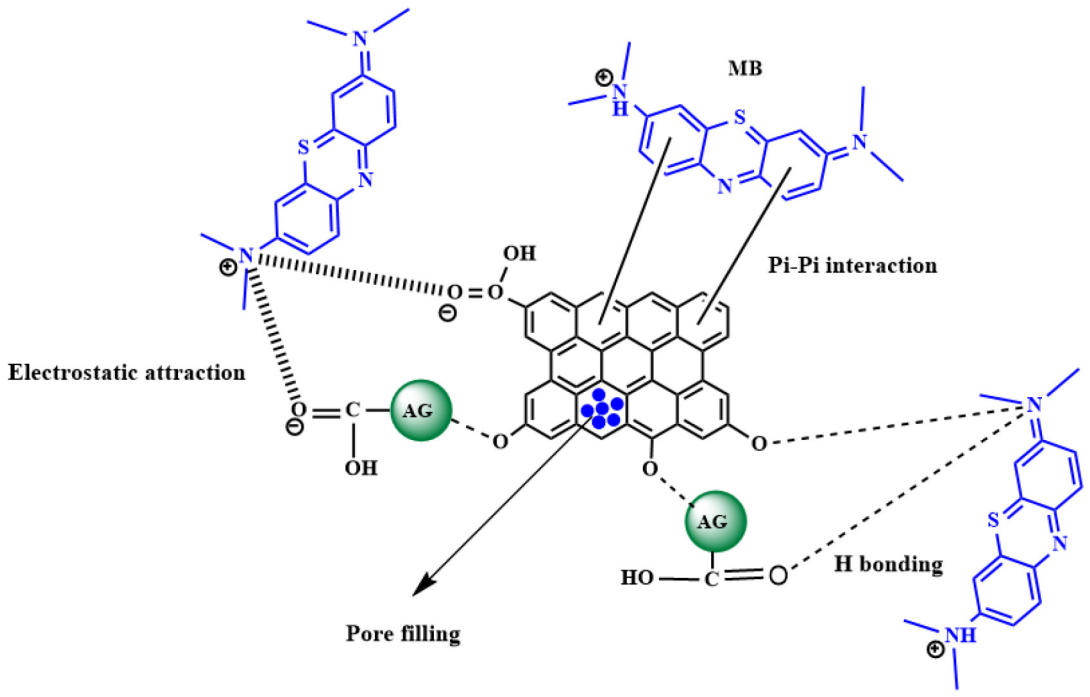

Fig. 12. A proposed mechanism of adsorption for the removal of MB dye onto CWDAG.

Table 9. Thermodynamic parameters of MB dye adsorption onto CWDAG.

Temperature (K)	K_d	ΔG° (kJ/mol)	ΔH° (kJ/mol)	ΔS° (J/mol.K)
298.15	2.72	−2.13	177.3	0.60
308.15	15.9	−8.15		
318.15	314.6	−14.2		
328.15	1441.3	−20.2		

of CDWAG (5.4 nm) possible to be occupied by the MB dye (1.43 nm) [84]. Moreover, the electrostatic attraction occurs based on the pH_{pzc} (point of zero charge) of CDWAG, where it carries a negative charge in a medium at pH values above its pH_{pzc}, based on the cation nature of MB. The other interaction that contributes to the adsorption of MB onto CWDAG is hydrogen bonding between the N-atoms of the MB dye and H-atom sites of CWDAG. Lastly, the interaction of π–π stacking is supported the favorable affinity of MB onto the surface of CWDAG because of donor-acceptor interactions between the arene structure of CWDAG and the aromatic MB dye.

4. Conclusion

The combination of wood dust (WD) and algae (AG) was successfully converted into eco-friendly mesoporous adsorbent (CWDAG) *via* microwave radiation and assisted by H_3PO_4 activation. The impregnation ratio was 2 g of CWDAG per 1 mL of H_3PO_4. The ANOVA analysis shows the reliability and applicability of the developed model with F-value = 107.08 and p-value < 0.0001. Moreover, the dual interaction of AB, AC, and BC is significant since the p-value of this variable interaction is less than 0.05. The equilibrium and kinetic analysis provides support that adsorption of MB dye onto CWDAG involves chemisorption onto a heterogeneous surface. The latter related to comparable best fit results for the Freundlich (R^2 = 0.92) and the Langmuir (R^2 = 0.89) models. The Langmuir isotherm model enables estimation of the q_{max} of CWDAG is (32.3 mg/g). Several contributions were involved in the adsorption process of MB dye onto CWDAG, including π–π stacking, H-bonding, electrostatic forces, and pore filling. The result of this research confirms the economic feasibility and effective adsorbent properties of CWDAG for removal of cationic dyes. Future applications include studies of this adsorption technology to recover heavy metal ions, pesticides, phenolic chemicals, and pharmaceuticals from wastewater.

Acknowledgement

The authors would like to thank the Faculty of Applied Sciences, Universiti Teknologi MARA (UiTM) for research facilities. The author (Raja Razuan Raja Deris) is thankful to Research Management

Center (RMC), Universiti Teknologi MARA for Grean Penyelidikan Khas 2020 (GPK). The author (Ruihong Wu) is grateful to Hengshui University for its scientific research funding (2024XJPY01).

Funding

The author (Raja Razuan Raja Deris) is thankful to Research Management Center (RMC), Universiti Teknologi MARA for Grean Penyelidikan Khas 2020 (GPK). The author (Ruihong Wu) is grateful to Hengshui University for its scientific research funding (2024XJPY01).

Ethical approval

Not applicable.

Conflict of interests

The authors declare no conflict of interest.

Data availability

All data for this research has been included as tabular or graphic results in this article.

Author contributions

Raja Razuan Raja Deris; Conceptualization, Resources, Hazierul F. Awang; Formal analysis, Validation. Muhammad Hakim Azman; Formal analysis, Data Curation, Methodology. Intan Nur Hidayah Abdul Rashid; Formal analysis, Data Curation, Methodology. Ahmad Hapiz; Methodology, Writing Original. Ruihong Wu; Validation, Data Curation. Abdallah Reghioua; Data Curation, Methodology. Zaher Mundher Yaseen; Visualization, Validation. Lee D. Wilson; Lee D. Wilson; Validation, Writing - Review & Editing.

References

1. Zhao B, Sun X, Wang L, Zhao L, Zhang Z, Li J. Adsorption of methyl orange from aqueous solution by composite magnetic microspheres of chitosan and quaternary ammonium chitosan derivative. *Chin. J. Chem. Eng.* 2019;27:1973–1980.
2. Wang X, Zhang P, Xu F, Sun B, Hong G, Bao L. Adsorption of methylene blue on azo dye wastewater by molybdenum disulfide nanomaterials. *Sustainability*. 2022;14(13):7585.
3. Bensalah J, Berradi M, Habsaoui A, Dagdag O, El Amri A, El Khattabi O, Lebkiri A, Rifi EH. Adsorption of the orange methyl dye and lead (II) by the cationic resin Amberlite®IRC-50: Kinetic study and modeling of experimental data. *J. Chem. Soc. Pakistan.* 2021;43:535.
4. Bensalah J, Berradi M, Habsaoui A, Allaoui M, Essebaai H, El Khattabi O, Lebkiri A, Rifi EH. Kinetic and thermodynamic study of the adsorption of cationic dyes by the cationic artificial resin Amberlite®IRC50. *Mater. Today: Proc.* 2021;45:7468–7472.
5. Azam K, Shezad N, Shafiq I, Akhter P, Akhtar F, Jamil F, Shafique S. A review on activated carbon modifications for the treatment of wastewater containing anionic dyes. *Chemosphere*. 2022;306:135566.
6. Sultana M, Rownok MH, Sabrin M, Rahaman MH, Alam SN. A review on experimental chemically modified activated carbon to enhance dye and heavy metals adsorption. *Clean. Eng. Technol.* 2022;6:100382.
7. Ramutshatsha-Makhwedzha D, Mavhungu A, Moropeng ML, Mbaya R. Activated carbon derived from waste orange and lemon peels for the adsorption of methyl orange and methylene blue dyes from wastewater. *Heliyon*. 2022;8:09930.
8. Surender S, Balakumar S. Insight into the melamine-derived freeze-dried nanostructured g-C_3N_4 for expeditious photocatalytic degradation of dye pollutants. *Diam. Relat. Mater.* 2022;128:109269.
9. Aryee AA, Gao C, Han R, Qu L. Functionalized magnetic biocomposite based on peanut husk for the efficient sequestration of basic dyes in single and binary systems: Adsorption mechanism and Antibacterial study. *J. Environ. Chem. Eng.* 2022;10:108205.
10. Ihaddaden S, Aberkane D, Boukerroui A, Robert D. Removal of methylene blue (basic dye) by coagulation-flocculation with biomaterials (bentonite and Opuntia ficus indica). *J. Water Proc. Engineering.* 2022;49:102952–102964.
11. Zaharia MM, Vasiliu AL, Trofin MA, Pamfil D, Bucatariu F, Racovita S, Mihai M. Design of multifunctional composite materials based on acrylic ion exchangers and $CaCO_3$ as sorbents for small organic molecules. *React. Funct. Polym.* 2021;166:104997–105012.
12. de Toledo WDMC, Pinheiro RA, Trava-Airoldi VJ, Corat EJ. Development of boron-doped diamond (BDD) deposited on carbon nanotubes (CNT) to form BDD/CNT structures relevant for electrochemical degradation. *Diam. Relat. Mater.* 2022;127:109159–1109170.
13. Reshadi MAM, Bazargan A, McKay G. A review of the application of adsorbents for landfill leachate treatment: Focus on magnetic adsorption. *Sci. Total Environ.* 2020;731:138863–138878.
14. Foroutan R, Mohammadi R, Ramavandi B, Bastanian M. Removal characteristics of chromium by activated carbon/$CoFe_2O_4$ magnetic composite and Phoenix dactylifera stone carbon. *Korean J. Chem. Eng.* 2018;35(11):2207–2219.
15. Surra E, Ribeiro RR, Santos T, Bernardo M, Mota JP, Lapa N, Esteves IA. Evaluation of activated carbons produced from maize cob waste for adsorption-based CO_2 separation and biogas upgrading. *J. Environ. Chem. Eng.* 2022;10(1):107065.
16. Lee CL, Chin KL, H'ng PS, Rashid U, Maminski M, Khoo PS. Effect of pretreatment conditions on the chemical–structural characteristics of coconut and palm kernel shell: A potentially valuable precursor for eco-efficient activated carbon production. *Environ. Technol. Innov.* 2021;21:101309.
17. Sahu JN, Karri RR, Jayakumar NS. Improvement in phenol adsorption capacity on eco-friendly biosorbent derived from waste Palm-oil shells using optimized parametric modelling of isotherms and kinetics by differential evolution. *Ind. Crops Prod.* 2021;164:113333.

18. Samiyammal P, Kokila A, Pragasan LA, Rajagopal R, Sathya R, Ragupathy S, Reddy VRM. Adsorption of brilliant green dye onto activated carbon prepared from cashew nut shell by KOH activation: Studies on equilibrium isotherm. *Environ. Res.* 2022;212:113497.
19. Peighambardoust SJ, Foroutan R, Peighambardoust SH, Khatooni H, Ramavandi B. Decoration of citrus limon wood carbon with Fe_3O_4 to enhanced Cd^{2+} removal: A reclaimable and magnetic nanocomposite. *Chemosphere*. 2021;282:131088.
20. Karri RR, Sahu JN, Jayakumar NS. Optimal isotherm parameters for phenol adsorption from aqueous solutions onto coconut shell based activated carbon: Error analysis of linear and non-linear methods. *J. Taiwan Institute Chem. Eng.* 2017;80:472–487.
21. Fang L, Song YG, Yuan XC, Luo SY, Yi CJ, Feng Y, Sun W. Steel slag assisted pyrolysis of biomass for the preparation of compound adsorbent. *J. Biobased Mater. Bioenergy*. 2019;13:722–726.
22. Gan WT, Gao LK, Zhan XX, Li J. Preparation of thiol-functionalized magnetic sawdust composites as an adsorbent to remove heavy metal ions. *RSC Adv.* 2016;6:37600–37609.
23. Wang H, Yuan XZ, Zeng GM, Leng LJ, Peng X, Liao KLL, Peng LJ, Xiao ZH. Removal of malachite green dye from wastewater by different organic acid modified natural adsorbent: Kinetics, equilibriums, mechanisms, practical application, and disposal of dye-loaded adsorbent. *Environ. Sci. Pollut. Res.* 2014;21:11552–11564.
24. Zhan YF, Yang L, Lan JW, Shang JJ, Chen SQ, Guan XM, Li WX, Lin SJ. Mussel-inspired polydopamine decorated pomelo peel as a durable biosorbent for adsorption of cationic dyes. *Cellulose*. 2021;28:453–470.
25. Gupta V, Agarwal A, Singh M, Singh NB. Kail sawdust charcoal: A low-cost adsorbent for removal of textile dyes from aqueous solution. *SN Appl. Sci.* 2019;1(10):1271.
26. Mercy B, Isaac W, Boateng and Nathaniel OB. Evaluation of adsorption of textile dyes by wood sawdust. *Research Journal of Physical and Applied Sciences*. 2014;3(1):006–014.
27. Batzias FA, Sidiras DK. Simulation of dye adsorption by beech sawdust as affected by pH. *J. Hazard. Mater.* 2007;141:668–679.
28. Dulman V, Cucu-Man S, Popa VI, Muresan R. Adsorption properties of beech wood sawdust related to some textile dyes. *Anal. St. Univ. "Al. I. Cuza" Iasi*. 2000;VIII:245–252.
29. Bilal M, Rasheed T, Sosa-Hernandez JE, ´Raza A, Nabeel F, Iqbal HMN. Biosorption: An interplay between marine algae and potentially toxic elements—a review. *Mar. Drugs*. 2018;16:65.
30. Elgarahy AM, Elwakeel KZ, Elshoubaky GA, Mohammad SH. Microwaveaccelerated sorption of cationic dyes onto green marine algal biomass. *Environ. Sci. Pollut. Res.* 2019;26:22704–22722.
31. Qulatein HA, Yılmaz MS. Preparation of low-cost and non-conventional macroalgae-based biosorbent for fast and effectively selective dye adsorption. *Mater. Chem. Phys.* 2023;303:127741.
32. Vetrivel SA, Diptanghu M, Ebhin MR, Sydavalli S, Gaurav N, Tiger KP. Green algae of the genus Spirogyra: A potential absorbent for heavy metal from coal mine water. *Remediation*. 2017;27(3):81–90.
33. Ozdemir G, Ceyhan N, Manav E. Utilization of an exopolysaccharide produced by Cryseomonasluteola TEM05 in alginate beads for adsorption of cadmium and cobalt ions. *Bio Tech*. 2005;96:1677–1682.
34. Sun W, Sun W, Wang Y. Biosorption of Direct Fast Scarlet 4BS from aqueous solution using the green-tide-causing marine algae Enteromorpha prolifera. *Spectrochim. Acta Part A: Molecul. Biomol. Spect.* 2019;223:117347.
35. Doğar Ç, Gürses A, Açıkyıldız M, Özkan E. Thermodynamics and kinetic studies of biosorption of a basic dye from aqueous solution using green algae Ulothrix sp. *Colloids Surf. B: Biointer.* 2010;76:279–285.
36. Foong SY, Liew RK, Yang Y, Cheng YW, Yek PNY, Mahari WAW, Lam SS. Valorization of biomass waste to engineered activated biochar by microwave pyrolysis: Progress, challenges, and future directions. *Chem. Eng. J.* 2020;389:124401.
37. Al-Qaessi F. Production of Activated Carbon from Date Stones by Using Zinc Chloride. *Energy Sources, Part A: Rec, Util, and Envi Effects*. 2010;32(10):917–930.
38. Wong S, Yac'cob NaN, Hassan O, Inuwa IM. From pollutant to solution of wastewater pollution: Synthesis of activated carbon from textile sludge for dye adsorption. *Chin. J. Chem. Eng.* 2018;26(4):870–878.
39. Sirajo L, Zaini MaZ. Adsorption of water pollutants using H_3PO_4-activated lignocellulosic agricultural waste: A mini review. *Tox Rev*. 2022;42(1):349–361.
40. Genli N, Kutluay S, Baytar O, ŞahiN Ö. Preparation and characterization of activated carbon from hydrochar by hydrothermal carbonization of chickpea stem: An application in methylene blue removal by RSM optimization. *Int. J. Phyto*. 2021;24(1):88–100.
41. Uçar S, Erdem M, Tay T, Karagöz S. Removal of lead (II) and nickel (II) ions from aqueous solution using activated carbon prepared from rapeseed oil cake by Na_2CO_3 activation. *Clean Technol. Environ. Policy*. 2014;17(3):747–756.
42. Chiang CH, Chen J, Lin JH. Preparation of pore-size tunable activated carbon derived from waste coffee grounds for high adsorption capacities of organic dyes. *J. Environ. Chem. Eng.* 2020;8(4):103929.
43. Li D, Wang Y, Jiaojiao Z, Wang J, Liu X, Tian Y, Zhang Z, Qiao Y, Ling W, Li J, Wen L. Drying before microwave-assisted H_3PO_4 activation to produce highly mesoporous activated carbons. *Mater. Lett.* 2018;230:61–63.
44. Farki NNaNLT, Abdulhameed AS, Surip SN, ALOthman ZA, Jawad AH. Tropical fruit wastes including durian seeds and rambutan peels as a precursor for producing activated carbon using H_3PO_4-assisted microwave method: RSM-BBD optimization and mechanism for methylene blue dye adsorption. *Int. J. Phytoremediation*. 2023;25(12):1567–1578.
45. Dalvand A, Nabizadeh R, Ganjali MR, Khoobi M, Nazmara S, Mahvi AH. Modeling of reactive blue 19 azo dye removal from colored textile wastewater using L-arginine-functionalized Fe_3O_4 nanoparticles: Optimization, reusability, kinetic and equilibrium studies. *J. Magnet. Magnet. Mater.* 2016;404:179–189.
46. Hu L, Peng Y, Wu F, Peng S, Li J, Liu Z. Tubular activated carbons made from cotton stalk for dynamic adsorption of airborne toluene. *J. Taiwan Inst. Chem. Eng.* 2017;80:399–405.
47. Sing KS. Reporting physisorption data for gas/solid systems with special reference to the determination of surface area and porosity (Recommendations 1984). *Pure Appl. Chem.* 1985;57(4):603–619.
48. Foroutan R, Peighambardoust SJ, Latifi P, Ahmadi A, Alizadeh M, Ramavandi B. Carbon nanotubes/β-cyclodextrin/MnFe2O4 as a magnetic nanocomposite powder for tetracycline antibiotic decontamination from different aqueous environments. *J. Environ. Chem. Eng.* 2021;9(6):106344.
49. Foroutan R, Peighambardoust SJ, Hemmati S, Ahmadi A, Falletta E, Ramavandi B, Bianchi CL. Zn^{2+} removal from the aqueous environment using a polydopamine/hydroxyapatite/

Fe_3O_4 magnetic composite under ultrasonic waves. *RSC Adv*. 2021;11(44):27309–27321.
50. Oyewo OA, Adeniyi A, Sitholé B, Onyango MS. Sawdust-based cellulose nanocrystals incorporated with ZnO nanoparticles as efficient adsorption media in the removal of methylene blue dye. *ACS Omega*. 2020;5(30):18798–18807.
51. Chowdhury ZZ, Karim MZ, Ashraf MA, Khalid K. Influence of carbonization temperature on physicochemical properties of biochar derived from slow pyrolysis of durian wood (Durio zibethinus) sawdust. *BioResources*. 2016. doi:10.15376/biores.11.2.3356.
52. Chen YW, Lee HV, Juan JC, Phang SM. Production of new cellulose nanomaterial from red algae marine biomass Gelidium elegans. *Carbohydr. Polym.* 2016;151:1210–1219.
53. Xu J, Chen L, Qu H, Jiao Y, Xie J, Xing G. Preparation and characterization of activated carbon from reedy grass leaves by chemical activation with H_3PO_4. *Appl. Surf. Sci.* 2014;320:674–680.
54. Adegoke KA, Adesina OO, Okon-Akan OA, Adegoke OR, Olabintan AB, Ajala OA, Olagoke H, Maxakato NW, Bello OS. Sawdust-biomass based materials for sequestration of organic and inorganic pollutants and potential for engineering applications. *CRGSC*. 2022;5:100274.
55. Almomani F, Bohsale RR. Bio-sorption of toxic metals from industrial wastewater by algae strains Spirulina platensis and Chlorella vulgaris: Application of isotherm, kinetic models and process optimization. *Sci. Total Environ.* 2021;755:142654.
56. Kutluay S, Temel F. Silica gel based new adsorbent having enhanced VOC dynamic adsorption/desorption performance. *Colloids Surf. A: Physicochem. Eng. Asp.* 2021;609:125848.
57. Foroutan R, Peighambardoust SJ, Mohammadi R, Peighambardoust SH, Ramavandi B. Development of new magnetic adsorbent of walnut shell ash/starch/Fe_3O_4 for effective copper ions removal: Treatment of groundwater samples. *Chemosphere*. 2022;296:133978.
58. Ashrafi SD, Safari GH, Sharafi K, Kamani H, Jaafari J. Adsorption of 4-Nitrophenol on calcium alginate-multiwall carbon nanotube beads: Modeling, kinetics, equilibriums and reusability studies. *Int. J. Biol. Macromol.* 2021;185:66–76.
59. Natarajan E, Ponnaiah GP. Optimization of process parameters for the decolorization of Reactive Blue 235 dye by barium alginate immobilized iron nanoparticles synthesized from aluminum industry waste. *Environ. Nanotechnol. Monit. Manage.* 2017;7:73–88.
60. Jayan N, Laxmi DBM, Akbar ST. Central composite design for adsorption of Pb(II) and Zn(II) metals on PKM-2 moringa oleifera leaves. *ACS Omega*. 2021;6(39):25277–25298.
61. Rose PK, Poonia V, Kumar R, Kataria N, Sharma P, Lamba J, Bhattacharya P. Congo red dye removal using modified banana leaves: Adsorption equilibrium, kinetics, and reusability analysis. *Groundw. Sustain. Dev.* 2023;23:101005.
62. Jawad AH, Sahu UK, Mastuli MS, ALOthman ZA, Wilson LD. Multivariable optimization with desirability function for carbon porosity and methylene blue adsorption by watermelon rind activated carbon prepared by microwave assisted H_3PO_4. *Biomass Conv. Bioref.* 2024;14:577–591.
63. Damiri F, Dobaradaran S, Hashemi S, Foroutan F, Vosoughi V, Sahebi S, Boffito DC. Waste sludge from shipping docks as a catalyst to remove amoxicillin in water with hydrogen peroxide and ultrasound. *Ultra. Sonochem.* 2020;68:105187.
64. Tang Y, Lin T, Jiang C, Zhao Y, Ai S. Renewable adsorbents from carboxylate-modified agro-forestry residues for efficient removal of methylene blue dye. *J. Phys. Chem. Solids*. 2021;149:109811.
65. Amin MT, Alazba AA, Shafiq M. Successful application of eucalyptus camdulensis biochar in the batch adsorption of crystal violet and methylene blue dyes from aqueous solution. *Sustain.* 2021;13(7):3600.
66. Lagergren S. Zur theorie der sogenannten adsorption geloster stoffe. *Vet. Akad. Handl.* 1898;24:1–39.
67. Ho YS, McKay G. Sorption of dye from aqueous solution by peat. *Chem. Eng. J.* 1998;70:115–124.
68. Theamwong N, Intarabumrung W, Sangon S, Aintharabunya S, Ngernyen Y, Hunt AJ, Supanchaiyamat N. Activated carbons from waste Cassia bakeriana seed pods as high-performance adsorbents for toxic anionic dye and ciprofloxacin antibiotic remediation. *Bioresour. Technol.* 2021;341:125832–125842.
69. Temkin MI. Kinetics of ammonia synthesis on promoted iron catalysts. *Acta physiochim. URSS*. 1940;12:327–356.
70. Frenudlich HMF. Over the adsorption in solution. *J. Phys. Chem.* 1906;57:385–471.
71. Langmuir I. The adsorption of gases on plane surfaces of glass, mica and platinum. *J. Am. Chem. Soc.* 1918;40:1361–1403.
72. Jin Y, Liu F, Li Y, Du Q, Song F, Chen B, Chen K, Zhang Y, Wang M, Sun Y, Zhao S, Jing Z, Pi X, Wang YQ, Wang D. Efficient adsorption of azo anionic dye Congo Red by micro-nano metal-organic framework MIL-68(Fe) and MIL-68(Fe)/chitosan composite sponge: Preparation, characterization and adsorption performance. *Int. J. Biol. Macromol.* 2023;252:126198.
73. Ramutshatsha-Makhwedzha D, Mavhungu A, Moropeng ML, Mbaya R. Activated carbon derived from waste orange and lemon peels for the adsorption of methyl orange and methylene blue dyes from wastewater. *Heliyon*. 2022;8(8): e09930.
74. Ghaedi M, Roosta M, Ghaedi AM, Ostovan A, Tyagi I, Agarwal S, Gupta VK. Removal of methylene blue by silver nanoparticles loaded on activated carbon by an ultrasound-assisted device: Optimization by experimental design methodology. *Res. Chem. Intermedi.* 2018;44(5): 2929–2950.
75. Yadav S, Dhakate SR, Singh BP. Carbon nanotube incorporated eucalyptus-derived activated carbon-based novel adsorbent for efficient removal of methylene blue and eosin yellow dyes. *Bioresour. Technol.* 2022;344(Pt B): 126231.
76. Misran E, Bani O, Situmeang EM, Purba AS. Banana stem-based activated carbon as a low-cost adsorbent for methylene blue removal: Isotherm, kinetics, and reusability, Alex. *Eng. J.* 2022;61(3):1946–1955.
77. Hapiz A, Jawad AH, Wilson LD, Abdulhameed AS, ALOthman ZA. Woody lignocellulosic waste conversion into activated carbon via microwave-assisted $ZnCl_2$ activation: Multivariable optimization for methylene blue dye removal. *Biomass Conversion and Biorefinery*. 2023. https://doi.org/10.1007/s13399-023-04868-5.
78. da Silva AI, Paranha G, Maia LS, Mulinari DR. Development of Activated Carbon from Pineapple Crown Wastes and Its Potential Use for Removal of Methylene Blue. *J. Nat. Fibers*. 2021;19(13):5211–5226.
79. Ao W, Fu J, Mao X, Wahab N, Ran C, Kang Q, Bi X. Characterization and analysis of activated carbons prepared from furfural residues by microwave-assisted pyrolysis and activation. *Fuel Process. Technol.* 2021;213:106640.
80. Durrani W, Nasrullah A, Khan A, Fagieh TM, Bakhsh EM, Akhtar K, Khan SB, Din IU, Khan MS, Bokhari A. Adsorption efficiency of date palm based activated carbon-alginate membrane for methylene blue. *Chemosphere*. 2022;302:134793.

81. Gao X, Xu D, Gao Y, Chen G, Zhai R, Huang X, Liu G. Mussel-inspired triple bionic adsorbent: Facile preparation of layered double hydroxide@ polydopamine@ metal-polyphenol networks and their selective adsorption of dyes in single and binary systems. *J. Hazard. Mater.* 2021;420:126609.
82. Al-musawi HA, Al-Mammar DE. Adsorption of Naphthol Green B Dye on to Ca-Montmorillonite and Nano-Composite Ca-Montmorillonite Clay. *Ann. Rom. Soc. Cell Biol.* 2021;25(5):2797–2810.
83. Ahmad R, Ansari K. Fabrication of alginate@ silver nanoparticles (Alg@AgNPs) bionanocomposite for the sequestration of crystal violet dye from aqueous solution. *Int. J. Biol. Macromol.* 2022;218:157–167.
84. Mahapatra U, Chatterjee A, Das C, Manna AK. Adsorptive removal of hexavalent chromium and methylene blue from simulated solution by activated carbon synthesized from natural rubber industry biosludge. *Environ. Technol. Innova.* 2021;22:101427.